



## Research article

# Exploring the mechanism of Huanglian ointment in alleviating wound healing after anal fistula surgery through metabolomics and proteomics

Dongliang Zhang<sup>a,c,1</sup>, Jiabo Gu<sup>a,b,1</sup>, Yanyan Xu<sup>b</sup>, Xiaowen Yu<sup>c</sup>, Heiying Jin<sup>b,\*</sup><sup>a</sup> Nanjing University of Chinese Medicine, Nanjing, 210023, China<sup>b</sup> Department of Colorectal and Anal Surgery, The Second Affiliated Hospital of Nanjing University of Chinese Medicine, Nanjing, 210011, China<sup>c</sup> Department of Colorectal and Anal Surgery, Zhenjiang Hospital Affiliated to Nanjing University of Chinese Medicine (Zhenjiang Hospital of Traditional Chinese Medicine), Zhenjiang, 212001, China

## ARTICLE INFO

## Keywords:

Anal fistula  
Wound healing  
*S. aureus*  
Huanglian ointment  
Proteomics  
Metabolomics

## ABSTRACT

Anal fistula is a common anal and intestinal disease. The wound of anal fistula surgery is open and polluting, which is the most difficult to heal among all surgical incisions. To investigate the mechanism of Huanglian ointment (HLO) on wound healing after anal fistula incision. The *S. aureus* infected wound in SD rats were used to imitate poor healing wound after anal fistula surgery. SD rats with wound sites (n = 24) were randomly divided into four groups (Control group, Model group, Potassium permanganate (PP) treatment group, and HLO treatment group). The wound healing rate was evaluated, HE staining was used to evaluate the pathological changes of each group, ELISA was used to detect the secretion of inflammatory factors in each group, and the mechanism was explored through metabolomics and proteomics in plasma rat. Compared to other groups, the rate of wound healing in the HLO group was higher on days 7 and 14. Histological analysis showed that collagen and fibroblast in HLO rats were significantly increased, inflammatory cells were reduced, and vascular endothelial permeability was increased. ELISA results showed that the secretion of inflammatory factors in HLO rats was significantly lower. Significant proteins and metabolites were identified in the wound tissues of the infected rats and HLO-treated rats, which were mainly attributed to Cdc42, Ctnnb1, Actr2, Actr3, Arpc1b, Itgam, Itgb2, Ctn, Linoleic acid metabolism, D-Glutamine and D-glutamate metabolism, Phenylalanine, tyrosine and tryptophan biosynthesis, Phenylalanine metabolism, alpha-Linolenic acid metabolism, and Ascorbate and aldarate metabolism. In conclusion, this study showed that HLO can promote *S. aureus* infected wound healing, and the data provide a theoretical basis for the treatment of wounds after anal fistula surgery with HLO.

## 1. Introduction

Anal fistula is a granulomatous channel connecting the anal canal or rectum to the skin around the anus, and is a prevalent ailment

\* Corresponding author. Department of Colorectal and anal surgery, The Second Affiliated Hospital of Nanjing University of Chinese Medicine, 121 Jiangjiayuan Road, Gulou District, Nanjing City, 210011, China.

E-mail address: [202050117@njucm.edu.cn](mailto:202050117@njucm.edu.cn) (H. Jin).

<sup>1</sup> They make the same contribution.

<https://doi.org/10.1016/j.heliyon.2024.e29809>

Received 17 September 2023; Received in revised form 23 March 2024; Accepted 15 April 2024

Available online 16 April 2024

2405-8440/© 2024 The Authors. Published by Elsevier Ltd. This is an open access article under the CC BY-NC-ND license (<http://creativecommons.org/licenses/by-nc-nd/4.0/>).

in the field of anal health [1]. Following the occurrence of an anal fistula, patients may experience frequent discharge of pus or fluids from the anal region, causing discomfort [2]. In cases of secondary infection, anal pain and eczema in the anal region may also be present [3]. Surgical intervention represents the sole curative approach for anal fistula [4]. Because of the special physiological function of daily defecation of the anus, the pollution is serious, so the anal fistula Surgical incision is generally not sutured, providing a good growth environment for exogenous microorganisms, thus causing bacterial infection [5]. Infections caused by surgical wounds account for a quarter of hospital-acquired infections, with surgical site infections comprising approximately 60–80 % of these cases. The infection rate is primarily determined by three factors: the extent of the surgery, the patient's resistance, and the degree of contamination at the wound site [6]. According to the report [7], surgical site infections are mainly caused by *Staphylococcus aureus*, *Escherichia coli* and *Enterococcus*. Currently, the most common treatment for bacterial infections is antibiotic therapy. However, with the increasing problem of antibiotic misuse, many bacteria have developed resistance, and infections caused by drug-resistant bacteria are particularly harmful to wounds and can even be life-threatening [8,9]. Therefore, there is an urgent need for local targeted dressings that possess good antimicrobial properties, minimal side effects, and no resistance. Additionally, inflammation is a major factor that limits normal wound healing. Inflammatory reactions induce a significant decrease in cell proliferation and differentiation, can trigger cell apoptosis, inhibit cell regeneration, and severely impact wound healing [10,11]. Furthermore, inflammation also inhibits angiogenesis, collagen deposition, and wound contraction [12]. Therefore, there is a pressing need for a wound dressing that can effectively reduce inflammation while providing antibacterial properties.

Natural medicines have been used in the treatment of infectious wounds due to their effectiveness, minimal toxic side effects, wide availability, and renewable nature [13]. "China Jianbing" is a composite wound nanomaterial composed of chitosan-polyvinyl alcohol (CTS-PVA) and propolis-poly- $\epsilon$ -caprolactone (PRO-PCL). In vitro, this composite nanomaterial effectively inhibits the growth of *Pseudomonas aeruginosa*, exhibits good antioxidant properties, and has hemostatic effects. In vivo, it suppresses inflammation, promotes collagen synthesis, and accelerates wound healing [14]. Jiang Tang Xiao Ke (JTXK), a traditional Chinese medicine formula, which promotes wound healing in *Staphylococcus aureus*-infected wounds by modulating miR-139-5p-mediated neutrophil proliferation and differentiation [15]. The Qingre Huayu (QRHY) Recipe promotes wound healing in a rat model of anal fistula surgery by reducing inflammation and increasing the number of collagen and fibroblast cells [16]. *Dracontomelon dao* promotes wound healing in *Escherichia coli*-induced wounds through its antimicrobial and anti-inflammatory activities, possibly by regulating the MAPK/NF- $\kappa$ B and PI3K/AKT signaling pathways [17]. Huanglian ointment (HLO) is an herbal combination containing *Coptis Rhizome*, *Chinese Angelica*, *Amur Corktree Bark*, *Rehmannia Root*, *Turmeric*, and *Sesame Oil*. It possesses the properties of clearing heat and toxins, eliminating dampness, alleviating discomfort, and accelerating the healing of wounds [18,19]. Currently, HLO has been used in our hospital for the treatment of wet wounds with significant clinical efficacy. Previous studies have identified 14 active compounds in HLO [18]. Both *Coptis Rhizome* and *Amur Corktree Bark* contain quercetin, a polyhydroxyflavonoid with antioxidant, free radical scavenging, anti-inflammatory, antimicrobial, antiviral, immune-regulatory, and cardiovascular protective effects, while decreasing neutrophil sensitivity to inflammatory factors [20]. Previous studies have shown that quercetin exhibits a good promoting effect on wound healing [21,22]. Wogonin in *Amur Corktree Bark* possesses broad biological activities, including antioxidant, anti-inflammatory, neuroprotective, antitumor, and antiviral activities [23]. Coptisine in *Coptis Rhizome* is an isoquinoline alkaloid with anticancer, antiarrhythmic, anti-inflammatory, antiviral, and lipid-lowering effects, also treating skin diseases by inhibiting the activity of lipoxygenase [24,25]. Demethoxycurcumin in *Turmeric* is one of the curcumin compounds that inhibits inflammatory mediators such as cyclooxygenase-2, lipoxygenase, tumor necrosis factor- $\alpha$ , interleukins, interferon- $\gamma$ , and nuclear transcription factor NF- $\kappa$ B, thereby exerting an anti-inflammatory effect [26]. Curcumin also exhibits excellent antibacterial effects and promotes wound healing [27,28]. However, there is limited research on the use of HLO in the healing of infectious wounds, and the relevant mechanisms are not yet clear.

Compound preparations in traditional Chinese medicine exhibit "multi-component, multi-target" effects by predominantly exerting pharmacological actions through complex systems and overall effects [29]. This poses significant difficulties for the investigation of Chinese herbal formulations. In the last few years, liquid chromatography-mass spectrometry (LC-MS) technology has rapidly advanced. LC-MS is widely utilized for proteomics and metabolomics research, including disease pathogenesis, drug target investigation, and biomarker identification [30,31]. The proteomic analysis of skin wounds treated with OCT demonstrated a noteworthy reduction in the levels of crucial agents implicated in tissue remodeling and re-epithelialization after injury. This includes significant decreases in pro-inflammatory cytokines (IL-8, IL-6) and matrix metalloproteinases (MMP1, MMP2, MMP3, MMP9), as opposed to the control samples [32]. Metabolomics by HPLC-MS/MS analysis showed Pien Tze Huang treatment significantly reversed multiple metabolites related to energy metabolism, such as glucose, glucuronic acid, inosine monophosphate, D-glucuronic acid, cis-aconitic acid, ribose-5-phosphate, and pantothenic acid, compared to diabetic wound rats [33]. In this study, we recreated the wound environment of a postoperative anal fistula by inducing acute inflammation in the wounds of rats. We investigated the promotive effect of HLO on wound healing via topical application and explored its potential mechanism through metabolomics and proteomics.

## 2. Method

### 2.1. Preparation of HLO

HLO is composed of *Coptis Rhizome*, *Chinese Angelica*, *Amur Corktree Bark*, *Rehmannia Root*, *Turmeric*, and *Sesame Oil*. These ingredients were purchased from the Affiliated Hospital of Zhenjiang Traditional Chinese Medicine University. The medicinal herbs (*Coptis Rhizome* 11.175 g, *Chinese Angelica* 18.625 g, *Amur Corktree Bark* 37.250 g, *Rehmannia Root* 11.175 g, and *Turmeric* 11.175 g, for a total of 89.4 g) were weighed and mixed with 447 g of *Sesame Oil*, soaked for 24 h, and fried at 200 °C for 4 h. The residue was then

removed. The concentration of HLO used in this study was 0.2 g/g [18].

## 2.2. Experimental animals and groups

24 healthy Sprague Dawley (SD) rats (male, 5–6 weeks, 140–170g) were used in the study, and the rats were purchased from the Si Pei Fu Biotechnology Co., Ltd, Beijing, China (Certificate Number: SCXK (JING) 2019–0010). During the experiment, they were fed standard feed and clean water, with regular adjustments to their feed, water, and bedding. Each rat was housed in a single cage, with an ambient temperature of 26 °C and alternating natural light exposure for 12 h. After a week of adaptive feeding, the experiment was performed. The animal experiments were approved by ethics association of the Wuhan Youdu Biotechnology Co., Ltd (Wuhan, China; approval no. WHYDSW20220606). The rats were fasted and denied water for 8 h before the operation. They were weighed and anesthetized with 2.5 % sodium pentobarbital (30 mg/kg) intraperitoneal (ip) injections [34–36]. After successful anesthesia, the rats were fixed in a prone position on an experimental platform with their back fur fully exposed. The surgical area was first shaved with an electric shaver and then depilated with hair removal cream. The skin layer on the right side of the spine of the rat was removed, causing a circular wound with a diameter of 2.0 cm that extended deep into the fascia. The wounds in 18 rats were soaked with 50 µL of *S. aureus* (ATCC6583, 10<sup>6</sup> CFU/mL) for 24 h to establish an experimental model of infection, and the wounds in 6 rats were treated with physiological saline as blank controls (Control). Subsequently, 18 rats with infected wounds were randomly divided into three groups: Model group (Model, n = 6), the wounds were soaked with 50 µL of *S. aureus* (ATCC6583, 10<sup>6</sup> CFU/mL) for 1 h, and then treated with physiological saline gauze; potassium permanganate (PP) treatment group (PP, n = 6), the wounds were soaked with 50 µL of *S. aureus* for 1 h, and then treated with potassium permanganate (a ratio of 1:5000 with water) gauze; Huanglian ointment treatment group (HLO, n = 6), the wounds were soaked with 50 µL of *S. aureus* for 1 h, and then treated with 0.2 g/g HLO. Dressing changes were performed once daily [16,37].

## 2.3. Specimen collection

After 14 days of treatment, rats were euthanized under anesthesia by intraperitoneal injection with pentobarbital sodium (150 mg/kg) [38,39]. The specimen collection process was performed under sterile conditions. The newly formed granulation tissue from the edge to the center of the wound, with a size of approximately 0.5 cm × 0.5 cm, was collected as a specimen. After successful specimen collection, it was immediately fixed in 4 % paraformaldehyde solution for 24 h, dehydrated, and embedded in paraffin. Serial sections of 4 µm were prepared.

## 2.4. HE staining

After dewaxing and rehydration, the sections were stained with hematoxylin for 10 min, washed with running water for 3 min, differentiated in 5 s of hydrochloric acid alcohol, washed with running water for 3 min, stained with eosin for 5 min, washed with running water for 5 s, dehydrated in graded alcohol, treated with xylene for transparency, and finally sealed with neutral gum. The specific pathological changes were observed and photographed using an optical microscope. Five random fields of view were observed and photographed, with images presented using 40X magnification.

## 2.5. Wound healing rate determination

The wound healing was observed on the 3rd, 7th and 14th day after treatment. Image J software was used for image processing to analyze the wound healing condition and calculate the wound healing rate. Wound healing rate (%) = (original wound area - unhealed wound area)/original wound area × 100 %.

## 2.6. ELISA

Mouse serum was extracted by centrifugation (4 °C, 15 min, 3500 rpm/min). The content of IL-6, TNF-α, and IL-1β in the serum was measured using IL-6 ELISA Kit (JYM0060Mo, ColorfulGene, Wuhan, China), TNF-α ELISA Kit (JYM0218Mo, ColorfulGene, Wuhan, China), and IL-1β ELISA Kit (JYM0531Mo, ColorfulGene, Wuhan, China), with specific steps outlined in the kit manual.

## 2.7. Blood sample processing

Fasting blood samples were collected in 5 mL Vacutainer tubes containing the chelating agent ethylene diamine tetraacetic acid (EDTA), then the samples were centrifuged for 15 min (1500 g, 4 °C). Each aliquot (150 µL) of the plasma sample was stored at –80 °C until LC-MS analysis. The plasma samples were thawed at 4 °C and 100 µL aliquots were mixed with 400 µL of cold methanol/ acetonitrile (1:1, v/v) to remove the protein. The mixture was centrifuged for 20 min (14000g, 4 °C). The supernatant was dried in a vacuum centrifuge. For LC-MS analysis, the samples were re-dissolved in 100 µL acetonitrile/water (1:1, v/v) solvent and centrifuged at 14000 g at 4 °C for 15 min, then the supernatant was injected.

## 2.8. UHPLC-QE-MS analysis

The analysis was conducted utilizing an UHPLC system (1290 Infinity LC, Agilent Technologies) integrated with a quadrupole time-of-flight instrument (AB SCIEX Triple TOF 6600) at Shanghai Applied Protein Technology Co., Ltd.

For the purpose of HILIC separation, the 2.1 mm × 100 mm ACQUITY UPLC BEH Amide 1.7 μm column (from waters, Ireland) was employed to analyze the samples. The separation parameters comprised of a column temperature of 25 °C, a flow rate of 0.5 mL/min, and an injection volume of 2 μL. The sample was maintained at 4 °C in an automated sampler throughout the analysis process. The mobile phase comprises two constituents: A and B. Constituent A is composed of water, 25 mM ammonium acetate, and 25 mM ammonia, while constituent B is acetonitrile. The gradient elution program commences with solvent B at a concentration of 95 % for the initial 0–0.5 min period, followed by a linear decline from 95 % to 65 % B during 0.5–7 min, another linear decline from 65 % to 40 % B during 7–8 min, and a constant concentration of 40 % B maintained from 8 to 9 min. Over the course of 0.1 min (9–9.1 min), the proportion of solvent B steadily increased from 40 % to 95 %. This 95 % ratio was sustained from 9.1 to 12 min.

The AB TripleTOF 6600 mass spectrometer was utilized to collect both MS1 and MS2 spectra for the sample. Following separation with the Agilent 1290 Infinity LC UHPLC system, mass spectrometric analysis was performed using the triple TOF 6600 mass spectrometer from AB SCIEX in both positive and negative ion modes, employing electrospray ionization (ESI). The ESI source parameters were configured with gas 1 and gas 2 at 60, the curtain gas (CUR) at 30 psi, the ion source temperature at 600 °C, and the spray voltage (ISVF) at ±5500 V (positive and negative modes). The mass-to-charge ratio ( $m/z$ ) range for primary mass detection was from 60 to 1000 Da, and the range for secondary sub-ion mass detection was from 25 to 1000 Da. The primary mass spectrometry scanning's accumulation time was 0.20 s per spectra, while the accumulation time of secondary mass spectrometry scanning was 0.05 s per spectra. The data-dependent acquisition (IDA) mode and the peak intensity value screening mode was used for the secondary mass spectrometry. The declustering potential (DP) was ±60 V (positive and negative modes), and the collision energy was 35 ± 15 eV. The IDA was configured with a dynamic exclusion range of 4 Da for isotopic ions and collected 10 fragment spectra per scan.

## 2.9. Metabolomics analysis

The original data were subjected to baseline filtering, peak identification, integration, retention time correction and peak alignment with the Progenesis QI (waters Corporation, Milford, USA), and finally a data matrix including retention time, mass to charge ratio and peak intensity was obtained. Then, the obtained data were imported into the multivariate statistical analysis software SIMCA-P11.0 (Umeteics, Umea, Sweden) for principal component analysis (PCA) and Orthogonal Partial Least Squares-Discriminant Analysis (OPLS-DA). After OPLS-DA analysis, take all values with VIP (variable importance in projection) value > 1 for significance statistical analysis. *t*-test is used for sample comparison between the two groups. The metabolites with VIP > 1 and *P* < 0.05 are potential biomarkers. Metlin database (<http://metlin.scripps.edu>), KEGG database (<http://www.kegg.com>) and HMDB (<http://www.hmdb.ca>) was used for the identification of the above metabolites, and undefined metabolites were deleted. MetaboAnalyst 5.0 (<https://www.metaboanalyst.ca/>) was used for enrichment analysis and pathway analysis.

## 2.10. Protein extraction and peptide enzymatic digestion

Samples (human, mouse, and rat serum samples need to remove serum high-abundance proteins first) were extracted with the SDT (4 % (w/v) SDS, 100 mM Tris/HCl pH7.6, 0.1 M DTT) lysis method for protein extraction and quantified using the BCA method. An appropriate amount of protein was taken from each sample using the Filter aided proteome preparation (FASP) method for trypsin digestion, and the peptides were desalted using a C18 cartridge, freeze-dried, and then resuspended in 40 μL of 0.1 % formic acid solution for peptide quantification (OD280).

## 2.11. LC-MS/MS analysis and data acquisition

Each sample was separated using the HPLC liquid system Easy nLC. Buffer A was a 0.1 % formic acid aqueous solution, while buffer B was a 0.1 % formic acid acetonitrile aqueous solution (acetonitrile was 84 %). Translation: "Chromatography column was balanced with 95 % A solution, and samples were automatically injected into the loading column (Thermo Scientific Acclaim PepMap100, 100 μm\*2 cm, nanoViper C18), followed by separation on the analysis column (Thermo scientific EASY column, 10 cm, ID75μm, 3 μm, C18-A2) at a flow rate of 300 nL/min.

Samples were analyzed by timsTOF Pro mass spectrometer after chromatographic separation. The detection mode was positive ion, and the ion source voltage was set to 1.5 kV. Both MS and MS/MS were detected and analyzed using TOF. The mass spectral scanning range was set to 100–1700  $m/z$ . The data acquisition mode used parallel accumulation serial fragmentation (PASEF), with 10 PASEF mode acquisitions of each level 1 mass spectrum and a cycle window time of 1.17 s. The dynamic exclusion time for tandem mass spectrometry was set to 24 s to avoid duplicate scans of ions.

## 2.12. The differential protein screening and bioinformatics analysis

"MaxQuant software (version 1.6.14) [7] was used for library identification and quantitative analysis of the raw data obtained from mass spectrometry analysis. The following parameters were used: Enzyme: Trypsin; Max Missed Cleavages: 2; Main Search: ±6 ppm; First Search: ±20 ppm; MS/MS Tolerance: 20 ppm; Fixed modifications: Carbamidomethyl (C); Variable modifications: Oxidation (M);

Database: uniprot\_rat\_33675\_20141101.fasta (33675 sequences, downloaded on November 11, 2014); Database Pattern: Reverse; Include Contaminants: True; Protein FDR:  $\leq 0.01$ ; Peptide FDR:  $\leq 0.01$ ; Peptides Used for Protein Quantification: Use Razor and Unique Peptides; Time Window (Match Between Runs): 2 min; Protein Quantification: LFQ; min. Ratio Count: 1. The unpaired *t*-test using R (version R4.0.3, <https://www.r-project.org/>) was used to analyze the difference in protein expression levels between Model and Control (Model\_vs\_Control) and between HLO and Model (HLO\_vs\_Model). Proteins with fold changes (FC)  $> 2$  (upregulated) or  $< 0.50$  (downregulated) and P value  $< 0.05$  were considered differentially expressed. The Venn diagram was used to determine the intersection between Model\_vs\_Control and HLO\_vs\_Model. The expression levels of the intersection proteins from the control, Model, and HLO groups were analyzed using pheatmap R package (1.0.12). The intersection proteins were analyzed for functional annotation using DAVID 6.8 (<https://david.ncifcrf.gov/tools.jsp>) for GO analysis and KEGG-PATHWAY pathway analysis. The STRING database

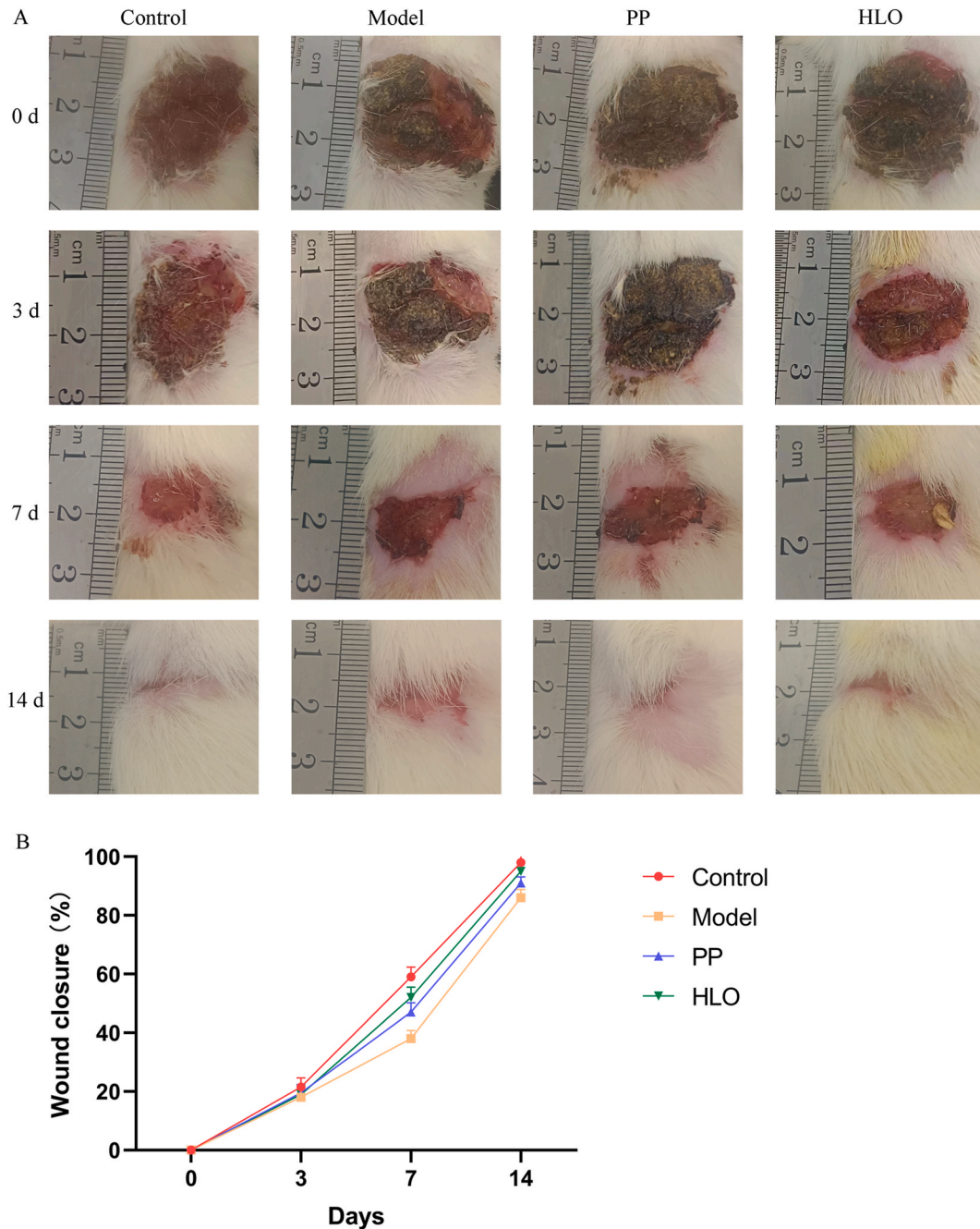


**Fig. 1.** HLO promoted the healing of infected wounds in rats. (A) On days 0, 3, 7, and 14, the wound healing status of rats in each group was displayed. (B) The wound healing rate in each group rat was calculated and analyzed.  $P < 0.01^{**}$  vs. Control group,  $P < 0.01^{##}$  vs. Model group.

(<http://string-db.org/>) was used to identify direct and indirect interactions between the intersection proteins. The Cytoscape software (version 3.2.1) was used to generate and analyze the interaction network.

### 2.13. Pearson correlation analysis

In metabolomics, metabolites related to metabolic pathways with an impact value  $> 0.2$  are screened. In proteomics, KEGG analysis showed that  $p < 0.05$  pathway-associated proteins were screened. Pearson correlation analysis was then performed on selected metabolites and proteins using the WGCNA R package. The results are displayed via the pheatmap R package. The correlation score is displayed by changes in color, with red representing positive correlation, blue representing negative correlation, and the darker the color, the stronger the correlation. In addition, the statistically significant ( $*p < 0.05$ ,  $**p < 0.01$ ,  $***p < 0.001$ ) is displayed in the corresponding area.

### 2.14. Statistical analysis

The experimental results were analyzed by SPSS 13 software. The obtained measurement data are expressed as mean  $\pm$  standard deviation (SD). Independent sample *t*-test was used to compare the mean between two groups, and one-way ANOVA was used to compare the mean between multiple groups.  $P < 0.05$  was statistically significant.

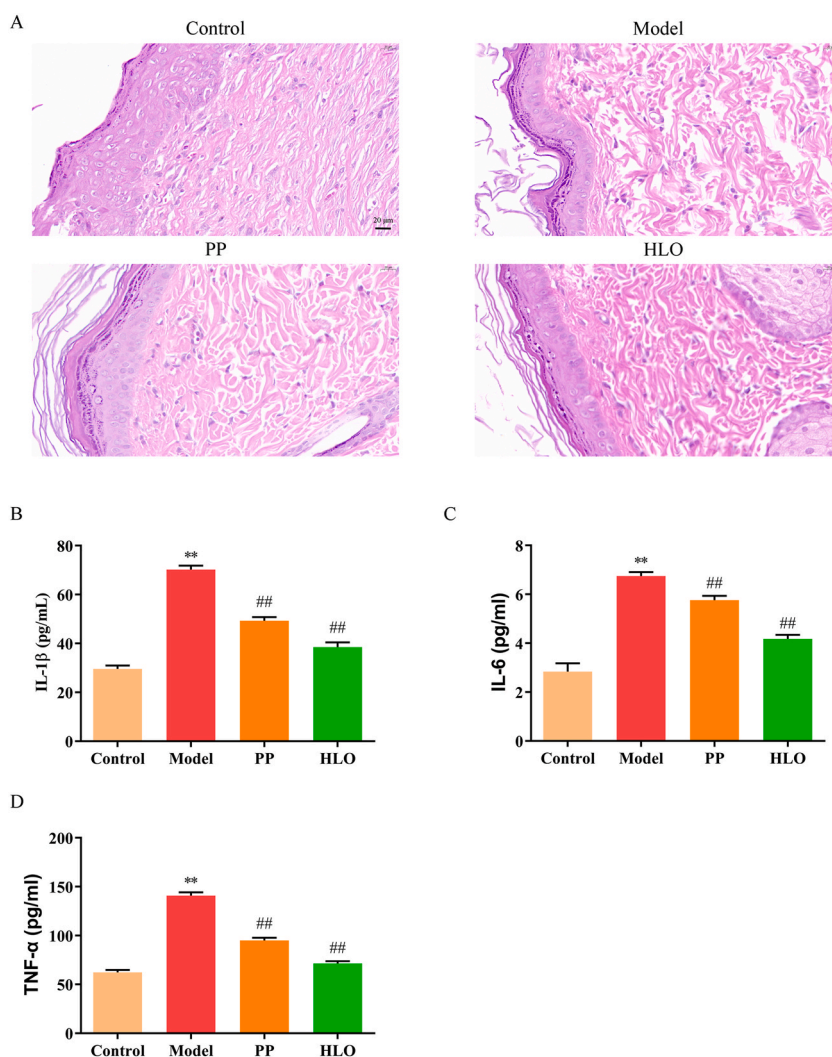


**Fig. 2.** The effect HLO on pathological changes in rat infected wounds and pro-inflammatory factors in serum at day 14. (A) HE staining was performed to measure the pathological changes of skin samples (magnification of 40X). (B) pro-inflammatory factors in serum were detected.  $P < 0.01^{**}$  vs. Control group,  $P < 0.01^{##}$  vs. Model group.

### 3. Results

#### 3.1. HLO promotes the healing of infected open wounds in rats

Wound healing conditions in each group of rats were observed at four time points: 0, 3, 7, and 14 days (Fig. 1A-B). No significant differences in wound healing rates were observed between the groups during the initial 3 days. Compared to the control group, wound healing in the model group was significantly slower on day 7 and day 14. Notably, wound healing in the HLO group was significantly faster than that in the model group, while progress was not evident in the PP group.

#### 3.2. HLO ameliorates histopathological changes and proinflammatory cytokine levels in rat infected open wounds

Pathological changes in wound tissue were observed on day 14. The wound tissue structure in the control group remained intact

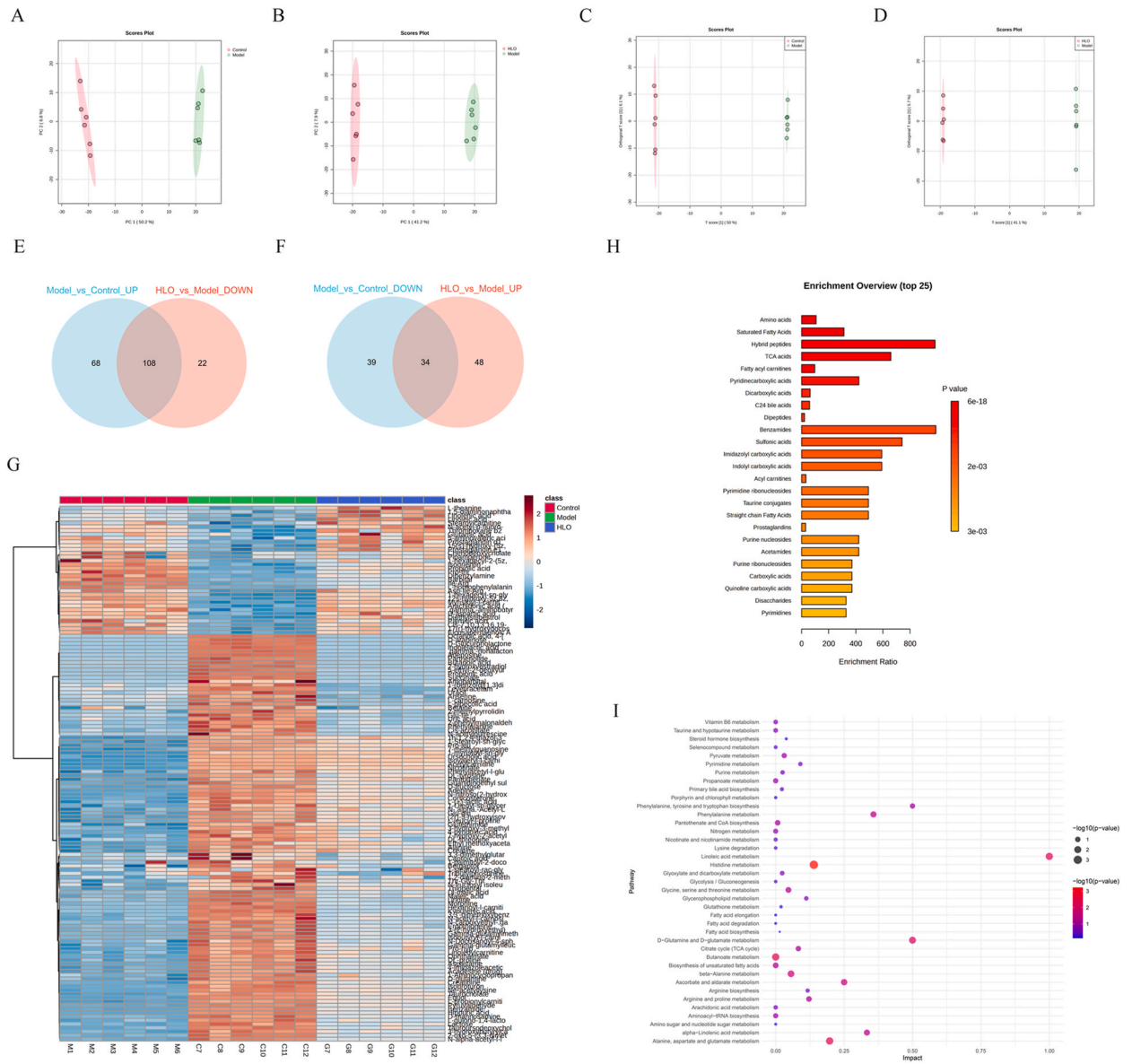


**Fig. 3. Metabolomics analysis.** (A) PCA score plot for the Control and Model groups. (B) PCA score plot for the HLO and Model groups. (C) OPLS-DA score plot for the Control and Model groups. (D) OPLS-DA score plot for the HLO and Model groups. (E) The venn analysis between upregulated metabolites in Model vs. Control and downregulated metabolites in Model vs. Control. (F) The venn analysis between downregulated metabolites in Model vs. Control and upregulated metabolites in Model vs. Control. (G) 142 metabolites from the results of venn analysis were showed through heatmap. (H) Top 25 of Enrichment analysis for 142 metabolites were showed. (I) Related pathway analysis of 142 metabolites were displayed.

without any abnormal changes. Compared to the control group, inflammatory cell infiltration increased, fibroblast decreased, and collagen fiber generation decreased in the model group wound. In contrast, inflammatory cell composition decreased, fibroblast increased, and collagen fiber generation increased in wounds of HLO and potassium permanganate (PP) groups. Moreover, the changes were more significant in the HLO group (Fig. 2A). In addition, the serum levels of proinflammatory cytokines (IL-1 $\beta$ , IL-6, TNF- $\alpha$ ) were measured on day 14 after successful establishment of the model. The results showed that the levels of IL-1 $\beta$ , IL-6, and TNF- $\alpha$  in all groups decreased during the treatment period, while the levels in the model group were significantly increased compared with those in the control group. However, the levels of IL-1 $\beta$ , IL-6 and TNF- $\alpha$  in the HLO and PP groups were significantly lower than those in the model group, and the decrease was more significant in the HLO group (Fig. 2B-D).

### 3.3. Metabolomics analysis

Untargeted metabolomics analysis was performed to investigate the effects of HLO on the healing of infected open wounds in rats. A total of 975 metabolites were identified using both positive and negative ion modes, with 613 and 362 metabolites identified in positive and negative ion modes, respectively. PCA and OPLS-DA were conducted to analyze the obtained mass spectrometry data, and the results showed a significant distance between the control and model groups, indicating that the model caused significant changes in endogenous substances from the basal state to the excited state. Similarly, a significant distance was observed between the HLO and model groups, indicating that HLO may have reversed the excited state back to the basal state (Fig. 3A-D). Significantly different metabolites were selected based on OPLS-DA VIP values > 1 and *p*-values < 0.05. A total of 176 upregulated metabolites and 73 downregulated metabolites were screened in the Model\_vs\_Control group, while 82 upregulated metabolites and 130 downregulated metabolites were screened in the HLO\_vs\_Model group (Fig. 3E-F). A Venn analysis was conducted to reveal the intersection of upregulated and downregulated metabolites between Model\_vs\_Control and HLO\_vs\_Model. A total of 108 and 34 common

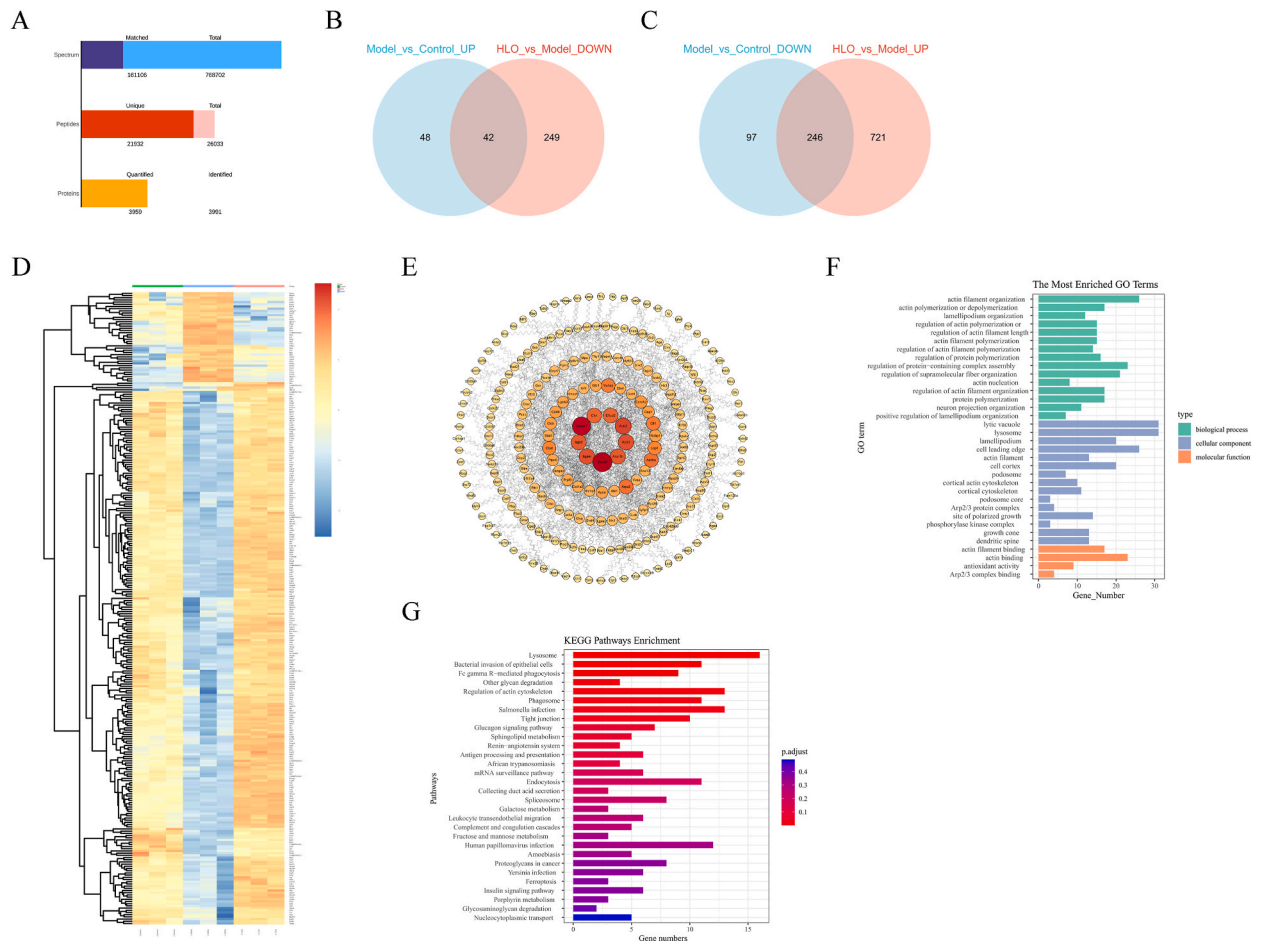


**Fig. 4. Proteomics analysis.** (A) Statistical histogram of identification and quantitative results. (B) The venn analysis between upregulated proteins in Model vs. Control and downregulated proteins in Model vs. Control. (C) The venn analysis between downregulated proteins in Model vs. Control and upregulated proteins in Model vs. Control. (D) 288 proteins from the results of venn analysis were showed through heatmap. (E) PPI analysis. (F) GO analysis. (G) KEGG analysis.

upregulated and downregulated metabolites were identified, respectively (Fig. 3E-F). Hierarchical clustering analysis of the 142 screened differentially expressed metabolites showed that the differences between the model group and the control group were mitigated by HLO treatment (Fig. 3G). The 142 differentially expressed metabolites were then imported into MetaboAnalyst 5.0, and 74 metabolites were identified for further enrichment and pathway analysis (Supplementary file 1). As Fig. 3H, The top 25 enrichment overview was showed, the results revealed that these metabolites were mainly enriched in amino acids, saturated fatty acids, hybrid peptides, TCA acids, fatty acyl carnitines, pyridinecarboxylic acids, dicarboxylic acids, C24 bile acids, dipeptides, benzamides, sulfonic acids, imidazolyl carboxylic acids, indolyl carboxylic acids, and acyl carnitines (Supplementary file 2). As Fig. 3I, the results of pathway analysis were showed. The pathway analysis identified six pathways with an impact >0.2, including linoleic acid metabolism, D-glutamine and D-glutamate metabolism, phenylalanine, tyrosine and tryptophan biosynthesis, phenylalanine metabolism, alpha-linolenic acid metabolism, and ascorbate and aldarate metabolism (Supplementary file 3). The metabolites associated with these pathways included linoleic acid, 1-palmitoyl-2-docosahexaenoyl-*sn*-glycero-3-phosphocholine, glutamic acid, D-glutamine, phenylalanine, hippuric acid, linolenic acid, L-gulonon-1,4-lactone, and D-glucuronolactone.

### 3.4. Proteomics analysis

The mechanism of action of HLO on the healing of infected open wounds in rats was further explored using proteomics. A total of 3991 proteins were identified, and 3959 proteins were quantified (Fig. 4A). In significantly different protein screening, 90 upregulated proteins and 343 downregulated proteins were selected from the Model\_vs\_Control group (Fig. 4B-C). After treatment with HLO, 967 proteins were upregulated and 291 proteins were downregulated compared to the model group (Fig. 4B-C). Venn analysis showed that 42 proteins were selected at the intersection of upregulated proteins in Model\_vs\_Control and downregulated proteins in HLO\_vs\_Model, and 246 proteins were selected at the intersection of downregulated proteins in Model\_vs\_Control and upregulated proteins in HLO\_vs\_Model (Fig. 4B-C). Clustering analysis showed that changes in 288 proteins screened (Supplementary file 4) in the model group were reversed by HLO (Fig. 4D). The 288 proteins screened were submitted to STRING website (<https://string-db.org/>) for PPI network construction and a total of 234 nodes and 649 edges were obtained (Fig. 4E). Nine genes including Cdc42, Ctnnb1, Actr2, Actr3, Arpc1b, Itgam, Itgb2, Eftud2, and Ctn were selected as the core PPI network (Fig. 4E). GO analysis of 288 screened proteins using DAVID 6.8 (<https://david.ncifcrf.gov/tools.jsp>) revealed a total of 97 significant entries, with 65 entries in the BP category, mainly including actin filament organization, actin polymerization or depolymerization, lamellipodium organization, regulation of actin polymerization or depolymerization, regulation of actin filament length, actin filament polymerization, regulation of actin filament polymerization, and regulation of protein polymerization. The CC classification includes 28 entries such as lytic vacuole, lysosome, lamellipodium, cell leading edge, and actin filament. The MF classification mainly includes 4 entries such as actin filament binding,

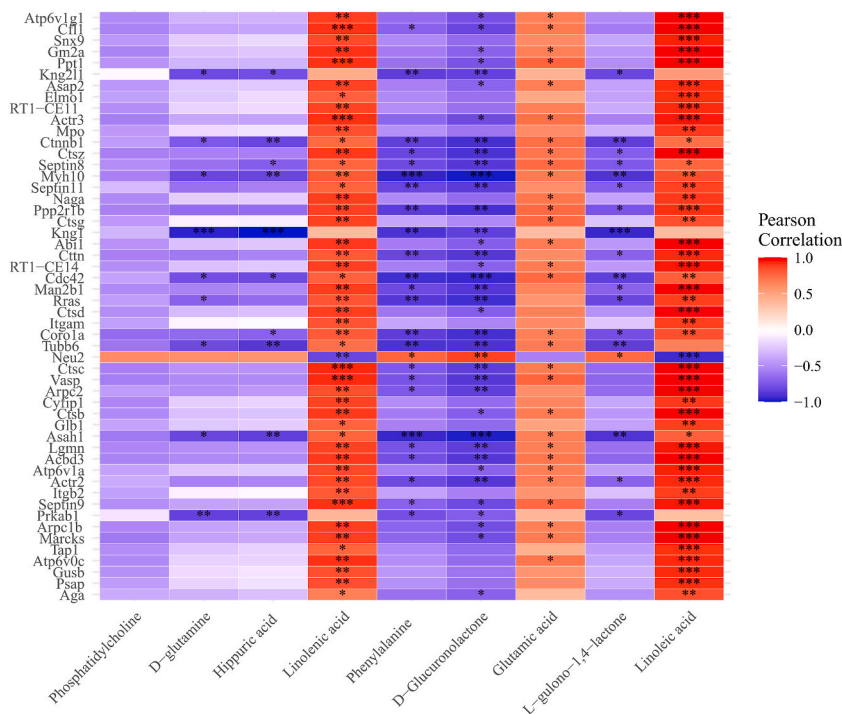


**Fig. 5.** Pearson correlation analysis of key metabolites and key proteins. The correlation score is displayed by changes in color, with red representing positive correlation, blue representing negative correlation, and the darker the color, the stronger the correlation. The correlation p-value is displayed in the corresponding area.

actin binding, antioxidant activity, and Arp2/3 complex binding (Supplementary file 5). The top 15, 15, and 4 entries with the smallest adjusted *p*-values for BP classification, CC classification, and MF classification are shown in Fig. 4F. In addition, KEGG enrichment analysis revealed 235 enriched signaling pathways, including Lysosome, Bacterial invasion of epithelial cells, Fc gamma R-mediated phagocytosis, other glycan degradation, Regulation of actin cytoskeleton, Phagosome, Salmonella infection, and Tight junction, and the top 30 pathways with the smallest adjusted *p*-values are shown in Fig. 4G. KEGG enrichment pathways of *p*-value <0.05 were showed in Supplementary file 6.

### 3.5. Pearson correlation analysis of key metabolites and proteins

9 metabolites (Linoleic acid, 1-palmitoyl-2-docosahexaenoyl-*sn*-glycero-3-phosphocholine (Phosphatidylcholine), Glutamic acid, *D*-glutamine, Phenylalanine, Hippuric acid, Linolenic acid, L-gulono-1,4-lactone, *D*-Glucuronolactone) were identified from 6 metabolic pathways (Impact >0.2) and 52 proteins (Aga, Psap, Gusb, Atp6v0c, Tap1, Marcks, Arpc1b, and Prkab1) were selected from 8 KEGG pathways (*p* < 0.05). The results showed that Linoleic acid, Linolenic acid, and Glutamic acid were positively correlated with these proteins, while Phosphatidylcholine, *D*-glutamine, Phenylalanine, Hippuric acid, L-gulono-1,4-lactone, and *D*-Glucuronolactone were negatively correlated with these proteins (Fig. 5).

## 4. Discussion

HLO contains multiple bioactive substances, which participate in the regulation of various pathways in many diseases [18,19,40]. However, there is still a lack of systematic analysis of the effect of HLO on the healing of anal fistula wounds after surgery. In our study, the potential mechanism of HLO in promoting the healing of anal fistula wounds after surgery was explored in a rat model of infectious open wounds. Our results confirmed that HLO can promote the healing of infectious open wounds in rats by increasing the healing rate, reducing the level of inflammatory factors, and increasing the number of fibroblasts and collagen fibers. We investigated the therapeutic mechanism of HLO through metabolomics and proteomics from a holistic and systematic perspective, which is applicable to various compounds, multiple targets, and multiple pathways in TCM.

The results of metabolomics analysis confirm that HLO promotes the healing of infected open wounds in rats by regulating the metabolisms of Linoleic acid, *D*-Glutamine and *D*-glutamate, Phenylalanine, tyrosine and tryptophan biosynthesis, Phenylalanine metabolism, alpha-Linolenic acid, and Ascorbate and aldarate. Linoleic acid, 1-palmitoyl-2-docosahexaenoyl-*sn*-glycero-3-phosphocholine (Phosphatidylcholine), Glutamic acid, *D*-glutamine, Phenylalanine, Hippuric acid, Linolenic acid, L-gulono-1,4-lactone, and *D*-Glucuronolactone are important metabolites in these pathways. Linoleic acid is a precursor to a series of biologically active compounds known as omega-6 fatty acids, and it is involved in regulating blood pressure, vascular reactivity, blood clotting, and the immune system [41]. Linoleic acid can increase the growth of keratinocyte and fibroblast cells, thereby promoting the healing of full-thickness burns [42]. Conjugated linoleic acid has been shown to promote wound healing in mice by reducing oxidative stress and the release of inflammatory factors [43]. Experiments at Heidelberg University Hospital have shown that purified Phosphatidylcholine has excellent anti-inflammatory properties and is a hydrophobic substance with great potential in the treatment of ulcerative colitis [44]. Glutamine is an important precursor to collagen synthesis, and collagen fibers have been shown to effectively promote wound healing [45]. *D*-glutamine is abundant in human serum and is a precursor to arginine, which can reduce the release of pro-inflammatory factors and enhance wound healing [46]. Phenylalanine is an aromatic amino acid with physiological activity. An increase in the concentration of Phenylalanine in serum is an indicator of rapid protein breakdown metabolism, which may be further up-regulated in sepsis with thermal injury [47]. Hippuric acid is a protein-bound uremic toxin mainly produced in the liver by the metabolism of benzoic acid [48]. Under normal circumstances, Hippuric acid can be excreted from the urine with a concentration in the serum of less than 5 mg/L. When an inflammatory reaction occurs in the body, the excretion of Hippuric acid is reduced, the concentration in the serum increases, and then stimulates the production of reactive oxygen species in vascular endothelial cells, further exacerbating the inflammatory response [49]. Alpha-linolenic acid is an unsaturated fatty acid that can be used to treat diabetes and eczema, and it has a promoting effect on wound healing as well [50,51]. L-gulono-1,4-lactone is a substrate for L-gulonoic acid- $\gamma$ -lactone oxidase, which promotes the last step of vitamin C synthesis. Therefore, L-gulono-1,4-lactone is regarded as the direct precursor of vitamin C, and a decrease in L-gulono-1,4-lactone indicates an increase in vitamin C synthesis [52]. Vitamin C has been shown to resist inflammation, increase immunity, and promote the healing of ulcers or wounds [53]. *D*-Glucuronolactone is a natural compound derived from glucose decomposition and has been reported to alleviate ochratoxin A-induced liver toxicity [54]. In our study, compared with the control group, Phosphatidylcholine, *D*-glutamine, Hippuric acid, Phenylalanine, *D*-Glucuronolactone, and L-gulono-1,4-lactone were up-regulated, and Linolenic acid and Linoleic acid were down-regulated in the model group of rats. However, treatment with HLO reversed these effects. Therefore, our study demonstrates that HLO promotes the healing of infected open wounds in rats by regulating Linoleic acid metabolism, *D*-Glutamine and *D*-glutamate metabolism, Phenylalanine, tyrosine and tryptophan biosynthesis, Phenylalanine metabolism, alpha-Linolenic acid metabolism, and Ascorbate and aldarate metabolism.

The analysis of proteomics revealed that 42 differentially expressed proteins were up-regulated in the model group and down-regulated in the HLO group, while 246 proteins were down-regulated in the model group and up-regulated in the HLO group. These proteins may be regulatory proteins involved in the process of improving wound healing in infected open wounds of rats treated with HLO. Results of protein-protein interaction (PPI) analysis showed that Cdc42, Ctnnb1, Actr2, Actr3, Arpc1b, Itgam, Itgb2, Eftud2, and Ctnn were core proteins. Furthermore, the KEGG enrichment analysis indicated that the therapeutics of HLO may be related to Lysosome (e.g., Aga and Psap), Bacterial invasion of epithelial cells (e.g., Arpc1b and Septin9), Fc gamma R-mediated phagocytosis (e.g., Marcks and Arpc1b), Other glycan degradation (e.g., Aga and Glb1), Regulation of actin cytoskeleton (e.g., Arpc1b and Itgb2),

Phagosome (e.g., Tap1 and Itgb2), Salmonella infection (e.g., Arpc1b and Acbd3), and Tight junction (e.g., Arpc1b and Prkab1). Taking the intersection of the 9 core proteins obtained from PPI analysis and the proteins identified in the KEGG enrichment analysis yielded 8 core proteins: Cdc42, Ctnnb1, Actr2, Actr3, Arpc1b, Itgam, Itgb2, and Ctnn. Cdc42, a member of the Rho GTPase family, plays a critical role in regulating the cytoskeleton of cells by controlling the formation of actin filamentous pseudopodia and directing cell migration, making it a key regulatory molecule in wound healing [55,56]. The Cdc42 signaling pathway is also involved in the migration of corneal epithelial cells and changes in cell cycle to repair wounds [57]. Moreover, it has been reported that during the invasion of endothelial cells by *S. aureus*, the aggregation of actin filaments recruits Cdc42GAP, which inactivates Cdc42 and terminates the aggregation of actin in the phagocytic cup [58]. The  $\beta$ -catenin encoded by Ctnnb1 is a multi-functional protein involved in cell adhesion and intercellular signal transduction. Previous studies have shown that  $\beta$ -catenin can promote the proliferation, differentiation, and migration of epidermal cells, thereby accelerating wound healing [59]. Research has shown that  $\beta$ -catenin is down-regulated in diabetic wounds, and up-regulation of  $\beta$ -catenin can promote healing of diabetic wounds [60]. Arpc1b, ACTR2, and ACTR3 are components of the Arp2/3 complex, which is involved in regulating a variety of cellular processes, including pseudopod formation, endocytosis, phagocytosis, and the formation of vesicular networks for loading cargoes of organelles such as the Golgi apparatus, the endoplasmic reticulum, and lysosomes [61]. The Arp2/3 complex is also involved in endothelial cell remodeling [62]. Itgam and Itgb2 encode integrin  $\alpha$ M and  $\beta$ 2 chains, respectively, which together form the leukocyte-specific integrin called Mac-1 [63]. Mac-1 deficiency leads to recurrent severe infections, impaired pus formation, and wound healing defects [64]. Ctnn, which encodes cortactin, a microfilament actin-binding protein, is involved in regulating the reshaping of the cytoskeleton. Ctnn can promote wound healing and improve endothelial cell damage [65]. Interestingly, these key proteins, including Cdc42, Ctnnb1, Actr2, Actr3, Arpc1b, Itgam, Itgb2, and Ctnn, were down-regulated in the model group and reversed by HLO treatment. These results further validate the role of HLO in improving the healing of infected open wounds in rats and provide potential mechanisms. In addition, the results of correlation analysis showed that these key proteins were highly correlated with the differentially metabolites of key pathways, thereby increasing the credibility of our study.

Anal fistula (chronic form of perianal abscess) is a disease that is difficult to treat clinically. In theory, a condition similar to a human perianal abscess can be created by inducing an infected wound on the back of a rat. However, this method has some limitations in simulating the specific pathological conditions of an anal fistula. On one hand, the cause of a human anal fistula is usually related to issues within the anal canal (such as infection of the anal rectal gland), rather than just skin or back infection. On the other hand, the anatomical location, pathological changes, and relationship with surrounding tissues of a human anal fistula are specific and may not be fully replicated in a rat model on the back.

In summary, HLO can promote the healing of infected wounds in rats and reduce inflammation. Our study found that the relevant mechanisms involved may include Linoleic acid metabolism, D-Glutamine and D-glutamate metabolism, Phenylalanine, tyrosine and tryptophan biosynthesis, Phenylalanine metabolism, alpha-Linolenic acid metabolism, and Ascorbate and aldarate metabolism. Additionally, HLO may be involved in regulating the healing of infected open wounds through the regulation of Cdc42, Ctnnb1, Actr2, Actr3, Arpc1b, Itgam, Itgb2, and Ctnn. This study provides a solid foundation for elucidating the mechanism of HLO in promoting the healing of infected wounds in anal fistula and provides new ideas for further research on the biomarkers of HLO efficacy.

## Funding

This work is supported by Jiangsu Province Traditional Chinese Medicine Technology Development Plan Project (Project No. YB201976); Zhenjiang Innovation Capacity Building Plan - Zhenjiang TCM Spleen and Stomach Disease Clinical Medical Research Center (Project No. SS2021005); Zhenjiang "Jinshan Talents" High level Leading Talent Training Plan (Phase VI "169 Project") Training Object Scientific Research Project.

## Ethics approval and consent to participate

Sprague Dawley rats were purchased from the Si Pei Fu Biotechnology Co., Ltd, Beijing, China (Certificate Number: SCXK (JING) 2019-0010). All animal experiments were conducted after an approval by the Institutional Animal Care and Use Committee at the Wuhan Youdu Biotechnology Co., Ltd (Wuhan, China; approval no. WHYDSW20220606). All methods were implemented in compliance with relevant guidelines and regulations. All methods are reported in accordance with the ARRIVE guidelines for the reporting of animal experiments, and comply with the American Veterinary Medical Association (AVMA) Guidelines for the Euthanasia of Animals (2020).

## Consent for publication

Not applicable.

## Availability of data and materials

Data will be made available on request.

## CRediT authorship contribution statement

**Dongliang Zhang:** Writing – review & editing, Writing – original draft, Project administration, Conceptualization. **Jiabo Gu:** Resources, Investigation, Formal analysis, Data curation. **Yanyan Xu:** Resources, Investigation, Data curation. **Xiaowen Yu:** Methodology, Investigation, Formal analysis. **Heiying Jin:** Writing – review & editing, Writing – original draft, Project administration, Funding acquisition, Conceptualization.

## Declaration of competing interest

The authors declare that they have no known competing financial interests or personal relationships that could have appeared to influence the work reported in this paper.

## Acknowledgements

Not applicable.

## Abbreviations

HLO	Huanglian ointment
PP	Potassium permanganate
LC-MS	liquid chromatography-mass spectrometry
SD	Sprague Dawley
ip	intraperitoneal
S	aureus Staphylococcus aureus
ELISA	Enzyme-Linked Immunosorbent Assay
UHPLC-QE-MS	Ultra High Performance Liquid Chromatography - Quadrupole Orbitrap Mass Spectrometry
HILIC	Hydrophilic Interaction Liquid Chromatography
PCA	principal component analysis
OPLS-DA	Orthogonal Partial Least Squares-Discriminant Analysis
KEGG	Kyoto Encyclopedia of Genes and Genomes
WGCNA	Weighted Gene Co-expression Network Analysis
Cdc42	Cell Division Cycle 42
Ctnnb1	Catennin Beta 1
Actr2	Actin-related protein 2
Actr3	Actin-related protein 3
Arpc1b	Actin-Related Protein 2/3 Complex Subunit 1B
Itgam	Integrin Subunit Alpha M
Itgb2	Integrin Subunit Beta 2
Eftud2	Elongation Factor Tu GTP Binding Domain Containing 2
Ctn	Cortactin
GO	Gene Ontology
BP	Biological Process
CC	Cellular Component
MF	Molecular Function

## Appendix A. Supplementary data

Supplementary data to this article can be found online at <https://doi.org/10.1016/j.heliyon.2024.e29809>.

## References

- [1] E. Limura, P. Giordano, Modern management of anal fistula, *World J. Gastroenterol.* 21 (1) (2015) 12–20, <https://doi.org/10.3748/wjg.v21.i1.12>.
- [2] Z. Mei, et al., Risk Factors for Recurrence after anal fistula surgery: a meta-analysis, *Int. J. Surg.* 69 (2019) 153–164, <https://doi.org/10.1016/j.ijso.2019.08.003>.
- [3] J. Sugrue, et al., Pathogenesis and persistence of cryptoglandular anal fistula: a systematic review, *Tech. Coloproctol.* 21 (6) (2017) 425–432, <https://doi.org/10.1007/s10151-017-1645-5>.
- [4] M. Pescatori, Surgery for anal fistulae: state of the art, *Int. J. Colorectal Dis.* 36 (10) (2021) 2071–2079, <https://doi.org/10.1007/s00384-021-03917-7>.
- [5] X. Li, et al., Research on high anal fistula: a bibliometric analysis, *Ann. Palliat. Med.* 10 (11) (2021) 11492–11503, <https://doi.org/10.21037/apm-21-3190>.
- [6] D.J. Leaper, C.E. Edmiston, World Health Organization: global guidelines for the prevention of surgical site infection, *J. Hosp. Infect.* 95 (2) (2017) 135–136, <https://doi.org/10.1016/j.jhin.2016.12.016>.

- [7] M.I. Koumu, et al., Surgical site infection Post-appendectomy in a tertiary hospital, Jeddah, Saudi Arabia, *Cureus* 13 (7) (2021) e16187, <https://doi.org/10.7759/cureus.16187>.
- [8] S. Homaeigohar, A.R. Boccaccini, Antibacterial biohybrid nanofibers for wound dressings, *Acta Biomater.* 107 (2020) 25–49, <https://doi.org/10.1016/j.actbio.2020.02.022>.
- [9] X. Yang, et al., Pharmaceutical intermediate-modified gold nanoparticles: against multidrug-resistant bacteria and wound-healing application via an electrospun scaffold, *ACS Nano* 11 (6) (2017) 5737–5745, <https://doi.org/10.1021/acsnano.7b01240>.
- [10] Z.Y. Lei, et al., Efficacy of *Aeschynomene indica* L. leaves for wound healing and isolation of active constituent, *J. Ethnopharmacol.* 228 (2019) 156–163, <https://doi.org/10.1016/j.jep.2018.08.008>.
- [11] R. Vinaik, et al., NLRP3 inflammasome activity is required for wound healing after burns, *Transl. Res.* 217 (2020) 47–60, <https://doi.org/10.1016/j.trsl.2019.11.002>.
- [12] V.A. Aneasha, et al., Topical bilirubin-deferoxamine hastens excisional wound healing by modulating inflammation, oxidative stress, angiogenesis, and collagen deposition in diabetic rats, *J. Tissue Viability* 31 (3) (2022) 474–484, <https://doi.org/10.1016/j.jtv.2022.04.009>.
- [13] A. Ahuja, J. Gupta, R. Gupta, Miracles of herbal phytomedicines in treatment of skin disorders: natural healthcare perspective, *Infect. Disord.: Drug Targets* 21 (3) (2021) 328–338, <https://doi.org/10.2174/1871526520666200622142710>.
- [14] H. Zhao, et al., "Jianbing" styling multifunctional electrospinning composite membranes for wound healing, *Front. Bioeng. Biotechnol.* 10 (2022) 943695, <https://doi.org/10.3389/fbioe.2022.943695>.
- [15] W. Zhang, et al., Inhibition of miR-139-5p by topical JTXK gel promotes healing of *Staphylococcus aureus*-infected skin wounds, *Cells Dev* 166 (2021) 203658, <https://doi.org/10.1016/j.cdev.2021.203658>.
- [16] J. Gao, et al., The effect of qingre Huayu Recipe on wound healing after anal fistulotomy in sprague-dawley rats, *Comput. Math. Methods Med.* 2022 (2022) 9397478, <https://doi.org/10.1155/2022/9397478>.
- [17] J. Wen, et al., Wound healing effects of drometolone on bacterial infection wounds in rats and its potential mechanisms under simulated space environment, *Evid Based Complement Alternat Med* 2022 (2022) 4593201, <https://doi.org/10.1155/2022/4593201>.
- [18] S. Wang, et al., Huanglian ointment alleviates eczema by maintaining the balance of c-Jun and JunB and inhibiting AGE-RAGE-mediated pro-inflammation signaling pathway, *Phytomedicine* 105 (2022) 154372, <https://doi.org/10.1016/j.phymed.2022.154372>.
- [19] X.F. Zhang, et al., [Effects of Huanglian ointment on wound healing of mice with full-thickness skin defect and the related mechanism], *Zhonghua Shaoshang Zazhi* 32 (12) (2016) 714–720, <https://doi.org/10.3760/cma.j.issn.1009-2587.2016.12.003>.
- [20] K. Yuan, et al., Quercetin alleviates rheumatoid arthritis by inhibiting neutrophil inflammatory activities, *J. Nutr. Biochem.* 84 (2020) 108454, <https://doi.org/10.1016/j.jnutbio.2020.108454>.
- [21] L. Zhou, et al., Electrospun chitosan oligosaccharide/polycaprolactone nanofibers loaded with wound-healing compounds of Rutin and Quercetin as antibacterial dressings, *Int. J. Biol. Macromol.* 183 (2021) 1145–1154, <https://doi.org/10.1016/j.ijbiomac.2021.05.031>.
- [22] G. Ajmal, et al., Ciprofloxacin HCl and quercetin functionalized electrospun nanofiber membrane: fabrication and its evaluation in full thickness wound healing, *Artif. Cells, Nanomed. Biotechnol.* 47 (1) (2019) 228–240, <https://doi.org/10.1080/21691401.2018.1548475>.
- [23] J.M. Dai, et al., Wogonin alleviates liver injury in sepsis through Nrf2-mediated NF- $\kappa$ B signalling suppression, *J. Cell Mol. Med.* 25 (12) (2021) 5782–5798, <https://doi.org/10.1111/jcmm.16604>.
- [24] Y. Liu, et al., Coptisine protects against hyperuricemic nephropathy through alleviating inflammation, oxidative stress and mitochondrial apoptosis via PI3K/Akt signaling pathway, *Biomed. Pharmacother.* 156 (2022) 113941, <https://doi.org/10.1016/j.biopha.2022.113941>.
- [25] L.T.H. Nguyen, et al., Coptisine alleviates imiquimod-induced psoriasis-like skin lesions and anxiety-like behavior in mice, *Molecules* 27 (4) (2022), <https://doi.org/10.3390/molecules27041412>.
- [26] R.R. Kotha, D.L. Luthria, Curcumin: biological, pharmaceutical, nutraceutical, and analytical aspects, *Molecules* 24 (16) (2019), <https://doi.org/10.3390/molecules24162930>.
- [27] D. Akbik, et al., Curcumin as a wound healing agent, *Life Sci.* 116 (1) (2014) 1–7, <https://doi.org/10.1016/j.lfs.2014.08.016>.
- [28] C. Mohanty, S.K. Sahoo, Curcumin and its topical formulations for wound healing applications, *Drug Discov. Today* 22 (10) (2017) 1582–1592, <https://doi.org/10.1016/j.drudis.2017.07.001>.
- [29] M. Ye, et al., Network pharmacology, molecular docking integrated surface plasmon resonance technology reveals the mechanism of Toujie Quwen Granules against coronavirus disease 2019 pneumonia, *Phytomedicine* 85 (2021) 153401, <https://doi.org/10.1016/j.phymed.2020.153401>.
- [30] R.F. Dubin, E.P. Rhee, Proteomics and metabolomics in kidney disease, including insights into etiology, treatment, and prevention, *Clin. J. Am. Soc. Nephrol.* 15 (3) (2020) 404–411, <https://doi.org/10.2215/cjn.07420619>.
- [31] P. Zhao, et al., Integration of transcriptomics, proteomics, metabolomics and systems pharmacology data to reveal the therapeutic mechanism underlying Chinese herbal Bufei Yishen formula for the treatment of chronic obstructive pulmonary disease, *Mol. Med. Rep.* 17 (4) (2018) 5247–5257, <https://doi.org/10.3892/mmr.2018.8480>.
- [32] S. Seiser, et al., Octenidine-based hydrogel shows anti-inflammatory and protease-inhibitory capacities in wounded human skin, *Sci. Rep.* 11 (1) (2021) 32, <https://doi.org/10.1038/s41598-020-79378-9>.
- [33] J. Zhang, et al., Intragastric administration of Pien Tze Huang enhanced wound healing in diabetes by inhibiting inflammation and improving energy generation, *Phytomedicine* 109 (2023) 154578, <https://doi.org/10.1016/j.phymed.2022.154578>.
- [34] R. Kato, P. Foëx, Myocardial protection by anesthetic agents against ischemia-reperfusion injury: an update for anesthesiologists, *Can. J. Anaesth.* 49 (8) (2002) 777–791, <https://doi.org/10.1007/bf03017409>.
- [35] C.T. Ho, et al., Antioxidative effect of polyphenol extract prepared from various Chinese teas, *Prev. Med.* 21 (4) (1992) 520–525, [https://doi.org/10.1016/0091-7435\(92\)90059-q](https://doi.org/10.1016/0091-7435(92)90059-q).
- [36] Y. Yang, et al., Effect of aminoguanidine on caspase-3 expression in rat retina after ischemia-reperfusion injury, *Int. J. Ophthalmol.* 4 (3) (2011) 259–261, <https://doi.org/10.3980/j.issn.2222-3959.2011.03.09>.
- [37] D. Mei, et al., PEGylated graphene oxide carried OH-CATH30 to accelerate the healing of infected skin wounds, *Int. J. Nanomed.* 16 (2021) 4769–4780, <https://doi.org/10.2147/ijn.s304702>.
- [38] Y.Y. Ji, et al., Ischemic preconditioning ameliorates intestinal injury induced by ischemia-reperfusion in rats, *World J. Gastroenterol.* 21 (26) (2015) 8081–8088, <https://doi.org/10.3748/wjg.v21.i26.8081>.
- [39] Z. Tang, et al., Salidroside inhibits renal ischemia/reperfusion injury-induced ferroptosis by the PI3K/AKT signaling pathway, *Exp. Ther. Med.* 26 (5) (2023) 507, <https://doi.org/10.3892/etm.2023.12206>.
- [40] L. Pan, et al., Network pharmacology and metabolomics study on the intervention of traditional Chinese medicine Huanglian Decoction in rats with type 2 diabetes mellitus, *J. Ethnopharmacol.* 258 (2020) 112842, <https://doi.org/10.1016/j.jep.2020.112842>.
- [41] S.S. Naughton, et al., Linoleic acid and the pathogenesis of obesity, *Prostag. Other Lipid Mediat.* 125 (2016) 90–99, <https://doi.org/10.1016/j.prostaglandins.2016.06.003>.
- [42] D. Zhao, et al., Walnut ointment promotes full-thickness burning wound healing: role of linoleic acid, *Acta Cir. Bras.* 37 (9) (2022) e370902, <https://doi.org/10.1590/acb370902>.
- [43] N.Y. Park, G. Valacchi, Y. Lim, Effect of dietary conjugated linoleic acid supplementation on early inflammatory responses during cutaneous wound healing, *Mediat. Inflamm.* 2010 (2010) 342328, <https://doi.org/10.1155/2010/342328>.
- [44] H. Schneider, et al., Lipid based therapy for ulcerative colitis-modulation of intestinal mucus membrane phospholipids as a tool to influence inflammation, *Int. J. Mol. Sci.* 11 (10) (2010) 4149–4164, <https://doi.org/10.3390/ijms11104149>.
- [45] E. Arribas-López, et al., The effect of amino acids on wound healing: a systematic review and meta-analysis on arginine and glutamine, *Nutrients* 13 (8) (2021) 2498, <https://doi.org/10.3390/nu13082498>.

- [46] M. Barchitta, et al., Nutrition and wound healing: an overview focusing on the beneficial effects of curcumin, *Int. J. Mol. Sci.* 20 (5) (2019) 1119, <https://doi.org/10.3390/ijms20051119>.
- [47] I. Al-Sadoon, et al., Serum concentrations of phenylalanine and tyrosine isomers in patients with acute coronary syndrome, *Pol. Arch. Intern. Med.* 131 (11) (2021) 16107, <https://doi.org/10.20452/pamw.16107>.
- [48] B. Nair, Final report on the safety assessment of benzyl alcohol, benzoic acid, and sodium benzoate, *Int. J. Toxicol.* 20 (Suppl 3) (2001) 23–50, <https://doi.org/10.1080/10915810152630729>.
- [49] G. De Simone, et al., Hippuric acid: could become a barometer for frailty and geriatric syndromes? *Ageing Res. Rev.* 72 (2021) 101466 <https://doi.org/10.1016/j.arr.2021.101466>.
- [50] D.C. Wu, M.P. Goldman, A topical anti-inflammatory healing regimen utilizing conjugated linolenic acid for use post-ablative laser resurfacing of the face: a randomized, controlled trial, *J Clin Aesthet Dermatol* 10 (10) (2017) 12–17. PMID: 29344315.
- [51] M. Martín, et al., Antisense-mediated depletion of potato leaf omega3 fatty acid desaturase lowers linolenic acid content and reduces gene activation in response to wounding, *Eur. J. Biochem.* 262 (2) (1999) 283–290, <https://doi.org/10.1046/j.1432-1327.1999.00382.x>.
- [52] J.A. Radzio, et al., L-Gulono-1,4-lactone oxidase expression rescues vitamin C-deficient Arabidopsis (vtc) mutants, *Plant Mol. Biol.* 53 (6) (2003) 837–844, <https://doi.org/10.1023/B:PLAN.0000023671.99451.1d>.
- [53] J.M. Pullar, A.C. Carr, M.C.M. Vissers, The roles of vitamin C in skin health, *Nutrients* 9 (8) (2017) 866, <https://doi.org/10.3390/nu9080866>.
- [54] C.A. Marsh, Metabolism of D-glucuronolactone in mammalian systems. Inhibitory properties of the products of D-glucuronolactone-dehydrogenase action, *Biochem. J.* 99 (1) (1966) 22–27, <https://doi.org/10.1042/bj0990022>.
- [55] D.M. Appledorn, et al., Rac1 and Cdc42 are regulators of HRasV12-transformation and angiogenic factors in human fibroblasts, *BMC Cancer* 10 (2010) 13, <https://doi.org/10.1186/1471-2407-10-13>.
- [56] M. Xu, et al., Vascular endothelial Cdc42 deficiency delays skin wound-healing processes by increasing IL-1 $\beta$  and TNF- $\alpha$  expression, *Am J Transl Res* 11 (1) (2019) 257–268. PMID: 30787984.
- [57] S. Pothula, H.E. Bazan, G. Chandrasekher, Regulation of Cdc42 expression and signaling is critical for promoting corneal epithelial wound healing, *Invest. Ophthalmol. Vis. Sci.* 54 (8) (2013) 5343–5352, <https://doi.org/10.1167/iovs.13-11955>.
- [58] L. Rauch, et al., Staphylococcus aureus recruits Cdc42GAP through recycling endosomes and the exocyst to invade human endothelial cells, *J. Cell Sci.* 129 (15) (2016) 2937–2949, <https://doi.org/10.1242/jcs.186213>.
- [59] T. Ma, et al., Adipose mesenchymal stem cell-derived exosomes promote cell proliferation, migration, and inhibit cell apoptosis via Wnt/ $\beta$ -catenin signaling in cutaneous wound healing, *J. Cell. Biochem.* 120 (6) (2019) 10847–10854, <https://doi.org/10.1002/jcb.28376>.
- [60] Y. Xiong, et al., Circulating exosomal miR-20b-5p inhibition restores Wnt9b signaling and reverses diabetes-associated impaired wound healing, *Small* 16 (3) (2020) e1904044, <https://doi.org/10.1002/smll.201904044>.
- [61] J.V. Abella, et al., Isoform diversity in the Arp2/3 complex determines actin filament dynamics, *Nat. Cell Biol.* 18 (1) (2016) 76–86, <https://doi.org/10.1038/ncb3286>.
- [62] Y. Li, et al., Interaction of cortactin and Arp2/3 complex is required for sphingosine-1-phosphate-induced endothelial cell remodeling, *Exp. Cell Res.* 298 (1) (2004) 107–121, <https://doi.org/10.1016/j.yexcr.2004.03.023>.
- [63] M. Herb, A. Gluschko, M. Schramm, LC3-associated phagocytosis initiated by integrin ITGAM-ITGB2/Mac-1 enhances immunity to *Listeria monocytogenes*, *Autophagy* 14 (8) (2018) 1462–1464, <https://doi.org/10.1080/15548627.2018.1475816>.
- [64] L. Chen, et al., Wound healing in Mac-1 deficient mice, *Wound Repair Regen.* 25 (3) (2017) 366–376, <https://doi.org/10.1111/wrr.12531>.
- [65] S. Choi, et al., A genetic variant of cortactin linked to acute lung injury impairs lamellipodia dynamics and endothelial wound healing, *Am. J. Physiol. Lung Cell Mol. Physiol.* 309 (9) (2015) L983–L994, <https://doi.org/10.1152/ajplung.00062.2015>.